

## Article

# First-Principles Study of the Effect of Sn Content on the Structural, Elastic, and Electronic Properties of Cu–Sn Alloys

Lingzhi Zhang <sup>1</sup>, Yongkun Li <sup>1,2,\*</sup>, Rongfeng Zhou <sup>1,2,\*</sup>, Xiao Wang <sup>1</sup>, Qiansi Wang <sup>1</sup>, Lingzhi Xie <sup>1</sup>, Zhaoqiang Li <sup>1</sup> and Bin Xu <sup>3</sup>

<sup>1</sup> Faculty of Material Science and Engineering, Kunming University of Science and Technology, Kunming 650093, China; zlz2694@163.com (L.Z.); wang\_xiao@kust.edu.cn (X.W.); wqs5248@163.com (Q.W.); 18315338611@163.com (L.X.); 18087147862@139.com (Z.L.)

<sup>2</sup> City College, Kunming University of Science and Technology, Kunming 650093, China;

<sup>3</sup> Chengdu Tonglin Casting Industrial Co., Ltd., Chengdu 610000, China; xubinyyy@126.com

\* Correspondence: liyongkun@kust.edu.cn (Y.L.); zhourfchina@hotmail.com (R.Z.)

**Abstract:** In order to explore the mechanism of the influence of Sn contents on the relevant properties of Cu–Sn alloys, the structure, elasticity, electronic, and thermal properties of Cu–Sn alloys doped with different proportions of Sn (3.125 at%, 6.25 at%, and 9.375 at%) were established using the first-principles calculation based on density functional theory. Firstly, their lattice constants and Sn concentration comply with Vegard's Law. From the mixing enthalpy, it can be seen that Sn atoms can be firmly dissolved in the Cu matrix, and the structure is most stable when the Sn content is 3.125 at%. In addition, the introduction of mismatch strain characterized their solid solution strengthening effect. The elastic and electronic properties showed that when the Sn content is 6.25 at%, the Cu–Sn alloy has the best plasticity and the highest elastic anisotropy; when the Sn content is 3.125 at%, the Cu–Sn alloy is the most stable and has stronger bulk and shear modulus, which was mainly due to a stronger Cu–Cu covalent bond. Finally, the Debye temperature, thermal conductivity, and melting point were calculated. It is estimated that the thermal conductivity of Cu–Sn alloy is relatively good when the Sn content is low.



**Citation:** Zhang, L.; Li, Y.; Zhou, R.; Wang, X.; Wang, Q.; Xie, L.; Li, Z.; Xu, B. First-Principles Study of the Effect of Sn Content on the Structural, Elastic, and Electronic Properties of Cu–Sn Alloys. *Crystals* **2023**, *13*, 1532. <https://doi.org/10.3390/cryst13111532>

Academic Editors: Khitouni Mohamed and Joan-Josep Suñol

Received: 25 September 2023

Revised: 18 October 2023

Accepted: 19 October 2023

Published: 24 October 2023



**Copyright:** © 2023 by the authors. Licensee MDPI, Basel, Switzerland. This article is an open access article distributed under the terms and conditions of the Creative Commons Attribution (CC BY) license (<https://creativecommons.org/licenses/by/4.0/>).

**Keywords:** first-principles; Cu–Sn alloys; solution strengthening; elastic properties; electronic properties

## 1. Introduction

As one of the important engineering structural materials, Cu–Sn (bronze) alloys have important application values in the fields of aerospace, marine, electrical appliances, and other fields due to their excellent wear resistance, corrosion resistance, thermal conductivity, and electrical conductivity, as well as sufficient strength and ductility [1–4]. The mechanical properties of Cu–Sn alloys are closely related to the content of the alloying element Sn. Due to different phase compositions, Cu–Sn alloys with different Sn content have different applications. When the Sn content is between 3 and 4 wt.%, it is mainly used for elastic components, wear-resistant parts, and antimagnetic parts; when the Sn content is between 5 and 11 wt.%, it is mainly used for bearings, shaft sleeves, turbines, etc. [5]. Therefore, Sn content is a key factor affecting the mechanical properties of Cu–Sn alloys.

In recent years, the first-principles calculations have become a powerful complement to solve the difficulties in the production and preparation process of Cu alloys and conduct extensive development and prediction of new Cu alloys, bridging the gap between theory and experiment. Wen et al. [6] studied the energy, elasticity, and electronic properties of Fe–Cu disordered solid solution alloys (Cu doping ratios of 25 at%, 37.5 at%, and 50 at%, respectively), and found that the elastic stability of Fe–Cu disordered solid solution was positively correlated with the Cu content. Zhou et al. [7] calculated key physical parameters such as elastic constants, bulk modulus, heat capacity, Debye temperature,

and volumetric thermal expansion coefficient of  $\text{Cu}_6\text{Sn}_5$  and  $\text{Cu}_5\text{Zn}_8$  alloy phases. The calculated results were in agreement with experimental data, indicating that both  $\text{Cu}_6\text{Sn}_5$  and  $\text{Cu}_5\text{Zn}_8$  alloy phases were elastic anisotropic, and that  $\text{Cu}_6\text{Sn}_5$  had a low bulk modulus. Rong et al. [8] calculated the elastic properties and anisotropy of  $\text{Cu}_3\text{Sn}$ , indicating that in-depth discussion of the anisotropy of intermetallic compounds with preferential growth and large volume fraction in the joint will be of great significance for accurately characterizing the mechanical behavior of the entire joint. In summary, the first-principles method can accurately study and predict the mechanical properties of copper alloys. However, currently, the calculation of Cu–Sn alloys mainly focuses on the specific phase structure of copper alloys, and there are few studies on the effect of Sn content on the properties and properties of copper alloy disordered solid solutions. Therefore, under the premise of ensuring the basic stability of the fcc structure, it is necessary to establish a model of Cu–Sn disordered solid solution to study the effect of tin solute on its related properties.

In this study, the phase stability, mechanical properties, and electronic properties of Cu–Sn alloys with Sn content of 3.125 at%, 6.25 at%, and 9.375 at% have been systematically studied using a first-principles calculation method. The lattice constant, mixing enthalpy, yield stress, elastic constant, elastic modulus, density of state, differential charge density, and Debye temperature were calculated. This provides a theoretical basis for the subsequent research on Cu–Sn alloys and the design, development, and wide application of new copper alloys. It is worth mentioning that, according to the Cu–Sn phase diagram, the solid solution limit of Sn in Cu matrix is 15.8 wt.% (9.2 at%) [9]. When the Sn content is greater than 15.8 wt.%, in addition to solid solution, the  $\delta$ -phase ( $\text{Cu}_{41}\text{Sn}_{11}$ ) occurs, which adversely affects the properties and applications of the material [10,11]. The generation of the  $\delta$ -phase should be avoided or reduced as much as possible in the practical production applications. Therefore, the  $\delta$ -phase was not discussed in this study.

## 2. Calculation Method and Details

The calculations were all performed using the CASTEP (Cambridge Serial Total-Energy Package) [12–14] code, which is based on the first-principles plane-wave pseudopotential method of density functional theory (DFT) [15] to perform quantum mechanical calculations. The ultrasoft pseudopotential (USPPs) was used to evaluate the interaction between valence electrons and ions. In this case, the valence electron configurations of Cu and Sn are  $3p^63d^{10}4s^1$  and  $4d^{10}5s^25p^2$ , respectively. In addition, the generalized gradient approximation (GGA) of Perdew–Burke–Ernzerhof (PBE) is used to approximate the effect of the exchange–correlation energy on the calculated results [16]. In this calculation,  $2 \times 2 \times 2$  supercells based on fcc structure were established by Perl Script enumeration of alloy structures. According to the Lowest Energy Principle, the stability models ( $\text{Cu}_{31}\text{Sn}$ ,  $\text{Cu}_{30}\text{Sn}_2$ , and  $\text{Cu}_{29}\text{Sn}_3$ ) of Cu–Sn alloys with Sn contents of 3.125 at%, 6.250 at%, and 9.375 at% were screened out, respectively, as shown in Figure 1 and Table 1. The detailed modelling methodology is shown in Appendix A.1.

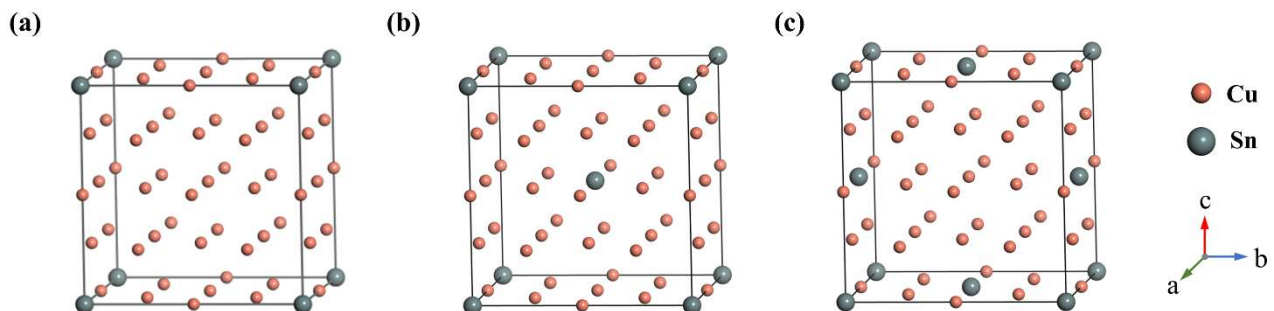


**Figure 1.** Crystal structure of Cu–Sn alloys (a)  $\text{Cu}_{31}\text{Sn}$ , (b)  $\text{Cu}_{30}\text{Sn}_2$ , and (c)  $\text{Cu}_{29}\text{Sn}_3$ .

**Table 1.** Cu–Sn alloys' model components.

Number of Sn Atoms	Structure	Mass Ratio of Sn Contents (wt.%)	Atomic Ratio of Sn Contents (at%)
0	Cu	0	0
1	Cu <sub>31</sub> Sn	5.864	3.125
2	Cu <sub>30</sub> Sn <sub>2</sub>	11.075	6.250
3	Cu <sub>29</sub> Sn <sub>3</sub>	16.195	9.375

The BFGS (Broyden–Fletcher–Goldfarb–Shanno) [17] minimization algorithm was then chosen to optimize these structures by full relaxation to bring the system to a more stable state. Then, after convergence tests, the maximum truncation energy of the plane wave basal energy was set to 450 eV, and the k-point sampling network in the Brillouin zone was generated based on the Monkhorst–Pack scheme and set to  $5 \times 5 \times 5$ . In the geometric optimization and electronic property calculations, the convergence tolerances for the total energy, maximum force, maximum stress, and maximum displacement were set to  $1 \times 10^{-5}$  eV/atom, 0.03 eV/Å, 0.05 GPa, and 0.001 Å. For the calculation of elastic properties, the convergence tolerances for total energy, maximum force, and maximum displacement were set to  $2 \times 10^{-6}$  eV/atom, 0.006 eV/Å, and  $2 \times 10^{-4}$  Å, respectively, and the number of steps and maximum strain amplitude for each strain were set to 4 and 0.003.

### 3. Results and Discussion

#### 3.1. Lattice Constant

The lattice constant can reflect the structure of the crystal and its internal composition, which is the basic parameter of the crystal structure and the basis for the study of the material structure [18]. The optimized lattice constants of Cu, Cu<sub>31</sub>Sn, Cu<sub>30</sub>Sn<sub>2</sub>, and Cu<sub>29</sub>Sn<sub>3</sub> are shown in Table 2. To verify the accuracy of the calculation results, the lattice constants of the pure copper model were compared with the experimental result [19] reported in other literature, which showed a difference of 0.387%. In general, the difference of the lattice constant is within 1%, which means that the obtained pseudopotential can be considered as a good pseudopotential [20], thus indicating that the model, conditions, and parameters are more reasonable. Figure 2 shows the calculated values of the lattice constant as a function of solute concentration, which was fitted linearly to obtain the following equation:

$$a (\text{Å}) = 3.629 + 1.144c \text{ with } R = 0.99995 \quad (1)$$

**Table 2.** Experimental and theoretical lattice parameters ( $a$ ,  $b$ ,  $c$  and  $\alpha$ ,  $\beta$ ,  $\gamma$ ), mixing enthalpy  $\Delta H$  (kJ/mol) for Cu–Sn alloys.

Structure	Source	$a$ (Å)	$b$ (Å)	$c$ (Å)	$\alpha$ (deg)	$\beta$ (deg)	$\gamma$ (deg)	$\Delta H$ (kJ/mol)
Cu	Exp. at 25 °C	3.615	-	-	90	-	-	[20]
	Present	3.629	-	-	90	-	-	
	Error	0.387%	-	-	-	-	-	
Cu <sub>31</sub> Sn	Present	3.664	-	-	90	-	-	−3.25
Cu <sub>30</sub> Sn <sub>2</sub>	Present	3.700	-	-	90	-	-	−2.69
Cu <sub>29</sub> Sn <sub>3</sub>	Present	3.736	-	-	90	-	-	−1.79

The result from E. Sidot [21] is also reported in Figure 2, where the same linear regression calculation was performed on these data. The relevant equation is as follows:

$$a (\text{Å}) = 3.615 + 1.054c \text{ with } R = 0.9997 \quad (2)$$

The results show that the lattice constants of Cu–Sn alloys are proportional to the solute concentration, in full compliance with Vegard's law. As can be seen from Figure 2, the calculated data agreed well with the slope of the experimental data, although the calculated results do not fully agree with the experimental results in terms of intercept

(equal to the lattice constant of pure Cu). The focus of this study is on the trend of lattice constant change, rather than the absolute value of lattice constant. The discrepancies between the calculated and experimental values of the pure Cu lattice constant are mainly due to thermal expansion and the limitations of the GGA [20]. Therefore, the optimized lattice constants can be used for subsequent calculations.

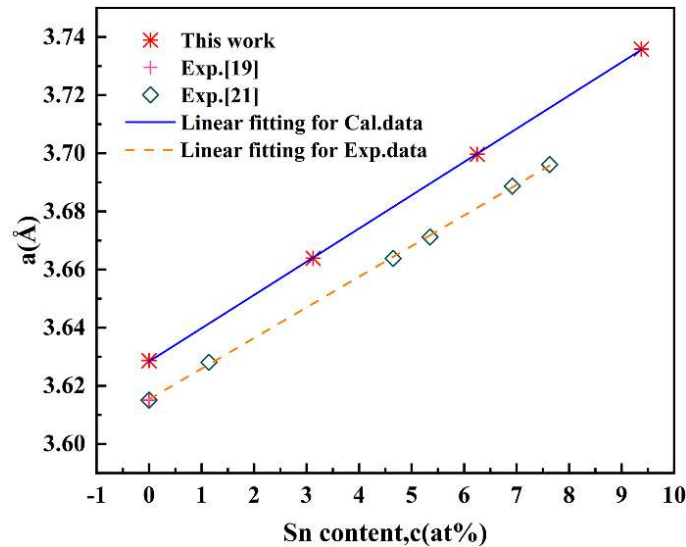


**Figure 2.** Relationship between the lattice parameter and the atomic Sn concentration of Cu–Sn alloys.

### 3.2. Enthalpy of Mixing

From the energy point of view, the mixing enthalpy  $\Delta H_{mixing}$  is usually introduced to describe the dissolution of the solute atom Sn in the Cu matrix, which expresses the relationship between the energies of two binary alloys with the same structure. However, the most stable structure of the element Sn in the ground state is not the fcc structure. The Birch–Murnaghan equation reveals the internal structure and properties of solids by investigating their rate of change of volume and modulus of elasticity at different pressures. The energy–volume ( $E$ - $V$ ) curve can be obtained by fitting this equation to obtain the total static energy of the pure element, which can then be substituted to obtain the enthalpy of mixing. In this calculation, in order to obtain the equilibrium volume  $V_0$  and the static energy  $E_0$  of the element Sn in the fcc structure, the energy–volume ( $E$ - $V$ ) curve in the ground state was fitted by the Birch–Murnaghan equation of state with the following empirical equation [22]:

$$E(V) = E_0 + \frac{9V_0B_0}{16} \left\{ \left[ \left( \frac{V_0}{V} \right)^{\frac{2}{3}} - 1 \right]^3 B'_0 + \left[ \left( \frac{V_0}{V} \right)^{\frac{2}{3}} - 1 \right]^2 \left[ 6 - 4 \left( \frac{V_0}{V} \right)^{\frac{2}{3}} \right] \right\} \quad (3)$$

where  $E_0$  and  $V_0$  are the static energy and equilibrium volume of each atom at steady state, respectively, while  $B_0$  and  $B'_0$  are the first-order derivatives of the bulk modulus and bulk modulus with respect to the pressure, respectively.

The enthalpy of mixing can then be calculated by the following equation:

$$\Delta H_{mixing}(Cu_xSn_y) = \frac{E_{total}(Cu_xSn_y) - xE_{atom}(Cu) - yE_{atom}(Sn)}{x + y} \quad (4)$$

where  $\Delta H_{mixing}(Cu_xSn_y)$ ,  $E_{total}(Cu_xSn_y)$ ,  $E_{atom}(Cu)$ , and  $E_{atom}(Sn)$  represent the mixing enthalpy, the static total energy of the Cu–Sn alloy, the static total energy of pure Cu and solute atom Sn, respectively, and  $x$  and  $y$  are the quantities of pure Cu and solute atom Sn, respectively.

Some scholars [23] pointed out that when evaluating the solid solubility of elements from the mixing enthalpy, if the contribution of entropy after heating is considered, there may be an uncertainty of approximately 0.05 eV/atom. It is shown that when the difference in radius between solute and solvent atoms  $|\Delta R| < 15\%$ , a solid solution with larger solid solution will be formed when other conditions are similar; conversely, when  $|\Delta R| > 15\%$ , the larger the  $|\Delta R|$ , and the smaller the solid solution. As for the electronegativity, if the difference in electronegativity between the group elements is small, a larger solid solution degree will be formed; if the difference is large, it is easier to form stable intermetallic compounds, and even if a solid solution can be formed, its solid solution degree is not large. In this study, the radius difference  $|\Delta R|$  between Cu and Sn is about 23.44%, which indicates a small solid solubility, while the electronegativity difference between the two is 0.06, indicating a large solid solubility. Therefore, the magnitude of solid solubility should be the result of a combination of multiple factors, which is related to the crystal structure, electron concentration, and temperature, in addition to the atomic size and electronegativity [24]. The more negative the mixing enthalpy, the stronger the chemical bond and the better the stability. As can be seen from Table 2, the mixing enthalpies of  $\text{Cu}_{31}\text{Sn}$ ,  $\text{Cu}_{30}\text{Sn}_2$ , and  $\text{Cu}_{29}\text{Sn}_3$  are all negative, and the negative value of the mixing enthalpy of  $\text{Cu}_{31}\text{Sn}$  is the largest, which is  $-3.25$  kJ/mol, indicating that 3.125 at%, 6.25 at%, and 9.375 at% Sn atoms can be solid-soluble in the Cu matrix, and  $\text{Cu}_{31}\text{Sn}$  (3.125 at%) has the strongest chemical bond and the most stable structure.

### 3.3. Solid Solution Strengthening

Substitution of some atoms in the copper-based solid solutions by solute atoms will cause lattice distortion. At this point, a strain field is formed around the solute atoms, which hinders the movement of dislocations, leading to solid solution strengthening [18]. Several mechanisms have been proposed to describe the interaction between mobile dislocations and solute atoms, including the size effect [25], modulus effect [26], Suzuki effect [27], and electrostatic interaction [28]. Among them, the size effect and the modulus effect are of more importance since the effect of solid solution strengthening of copper substrates is difficult to present in a quantitative form using conventional experimental methods. Therefore, in this study, based on first principles, we introduce the parameter mismatch strain, which is the local lattice distortion around the solute atom and the size effect mentioned earlier, as a measure of the strength of the solute atom strengthening by the characteristic strain generated by the size difference between some solute atoms represented by elastic inclusions and the pores of the host material in an elastic continuous medium model. The mismatch strain is defined as follows:

$$\varepsilon = \frac{d - d_0}{d_0} \quad (5)$$

where  $d$  is the distance between the host atom (Cu) and the first nearest neighbor of the solute atom (Sn), and  $d_0$  is the distance between the host atom (Cu) and the host atom (Cu). At zero pressure, the lattice constant is optimized to  $a_0$ , when the atomic positions are relaxed, and the distance  $d$  within the cell is measured. Then, the lattice constant is fixed to  $a_0$ , the atomic positions are fixed to the ideal fcc lattice position, and the distance  $d_0$  within the cell is measured. For the first nearest neighbor solvent atom, the relationship between  $d_0$  and the lattice constant is  $d_0 = a_0/\sqrt{2}$ . The mismatch strain  $\varepsilon$  for the first nearest neighbor in the Cu–Sn alloys is shown in Table 3. This parameter is determined based on the average value of the distance between the first nearest neighbor atoms in  $\text{Cu}_{31}\text{Sn}$ ,  $\text{Cu}_{30}\text{Sn}_2$ , and  $\text{Cu}_{29}\text{Sn}_3$  [20]. According to the Cottrell model [25], the maximum interaction force  $F_m$  between solute atoms and edge dislocations is:

$$F_m = \frac{\sqrt{3}}{2} \left( \frac{1 + \nu}{1 - \nu} \right) Gb^2 |\varepsilon| \quad (6)$$

where  $\nu$  is the Poisson's ratio,  $G$  is the shear modulus,  $b$  is the Burgers vector, and  $\varepsilon$  is the mismatch strain. In Friedel's theory [29], the interaction forces between atoms generate a critical decomposition shear stress  $\Delta\tau_s$ , which is defined as

$$\Delta\tau_s = \frac{\sqrt{2}F_m^{3/2}}{b^3} \sqrt{\frac{c}{G}} \quad (7)$$

where  $c$  is the concentration of solute atoms. Substituting  $F_m$  in Equation (6) into Equation (7) and then using the Taylor factor  $M$ , one obtains the yield stress  $\Delta\sigma_s$  increased by solid solution strengthening of the polycrystalline alloy with the following relation:

$$\Delta\sigma_s = M \frac{3^{3/4}}{2} \left( \frac{1+\nu}{1-\nu} \right)^{3/2} G |\varepsilon|^{3/2} \sqrt{c} \quad (8)$$

In Cu–Sn alloys, the value of  $M$  is 3.06 [30]. Table 3 summarizes the misfit strain  $\varepsilon$  induced by solid solution of Sn atom into the Cu matrix and the contribution of solid solution strengthening to the yield stress of Cu–Sn alloys. The Poisson's ratio  $\nu$  and shear modulus  $G$  in Equation (8) are obtained from Table 4; Table 5 below.

Figure 3 shows the relationship between the Sn content and the yield stress values in Cu–Sn alloys, comparing the calculated results with the analytical results of some experimental results [31–33]. The experimental values are distributed on both sides of the calculated results. In fact, the yield stress values depend on two major factors. On the one hand, it depends on the intrinsic factors of the material, including the bonding bonds and the influence of the microstructure dominated by four major strengthening mechanisms: solid solution strengthening, strain strengthening, dispersion strengthening, and grain size strengthening; on the other hand, the yield stress values are also affected by some extrinsic factors such as the temperature, the strain rate, and the state of stress [31]. As shown in Table 3, different processing methods and heat treatment conditions lead to different yield stress results when the solute atomic concentration is the same. The first-principles calculations used in this study simulate the relevant properties of the material at a nearly ideal 0 K condition, which differs from the experimental conditions. Hence, the yield strength values are somewhat deviated, but observing the overall trend in Figure 3, the yield stress values of the Cu–Sn alloys increase with the increase of the Sn content. The mismatch strain data obtained from this calculation, to a certain extent, can provide theoretical guidance for the solid solution strengthening effect of Cu–Sn alloys, which is of reference value for the development of new copper alloys with very high yield strength.

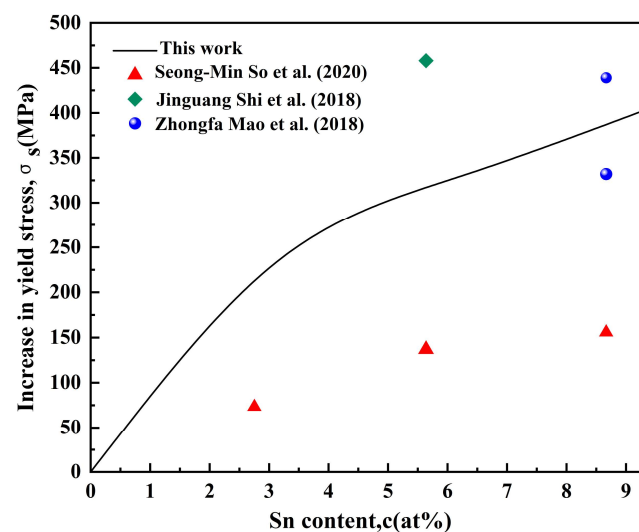


**Figure 3.** The relationship between the Sn content and the yield stress values in Cu–Sn alloys. This includes calculation results and experimental results [31–33].

**Table 3.** Theoretical results of mismatch strain caused by Sn atoms in Cu and the contribution of solution strengthening to the yield stress of Cu–Sn alloys. It also includes some solid solution strengthening experimental values.

	c (at%)	$\varepsilon$ (%)	$\Delta\sigma_s$ (MPa)	Notes
Present	3.125		233.52	
	6.25	1.97	330.24	
	9.375		404.46	
Exp.	2.753		68.5 ± 4.8	As-cast [31]
	5.639		133.4 ± 3.5	As-cast [31]
			458	SLM [32]
			139.2 ± 16.6	As-cast [31]
	8.668		436 ± 3	SLM [33]
		328 ± 4	SLM + annealing [33]	

### 3.4. Elastic Properties

The elastic constants of metallic materials usually express their mechanical properties, especially the stability and stiffness of the material [8]. They express the stress condition required to maintain a certain deformation.

In this study, the elastic constants will be obtained by the “stress-strain” method [34], and for cubic crystal, the system has three independent elastic constants:  $C_{11}$ ,  $C_{12}$ , and  $C_{44}$  [35].

Table 4 summarizes the elastic constants obtained from this calculation and compares the single-crystal elastic constants  $C_{ij}$  of pure Cu with the experimentally reported and previously calculated values. As can be seen from Table 4, the  $C_{ij}$  of  $\text{Cu}_{31}\text{Sn}$ ,  $\text{Cu}_{30}\text{Sn}_2$ , and  $\text{Cu}_{29}\text{Sn}_3$  do not satisfy the cubic crystal structure relationship because the number of independent elastic constants will increase after geometric optimization of the model obtained with supercell disordered modeling, whose crystal structure symmetry is slightly broken due to the quasi-random distribution of solute atoms. Therefore, in the present study, we used the symmetry-based projection (SBP) technique [36,37] to correct the elastic tensor of  $\text{Cu}_{31}\text{Sn}$ ,  $\text{Cu}_{30}\text{Sn}_2$ , and  $\text{Cu}_{29}\text{Sn}_3$ . We usually take the average of the relevant elastic parameters to obtain the elastic constants of these quasi-random systems [35]. The relation is as follows:

$$\overline{C_{11}} = \frac{(C_{11} + C_{22} + C_{33})}{3} \quad (9)$$

$$\overline{C_{12}} = \frac{(C_{12} + C_{13} + C_{23})}{3} \quad (10)$$

$$\overline{C_{44}} = \frac{(C_{44} + C_{55} + C_{66})}{3} \quad (11)$$

The average values of the relevant elastic parameters calculated for  $\text{Cu}_{31}\text{Sn}$ ,  $\text{Cu}_{30}\text{Sn}_2$ , and  $\text{Cu}_{29}\text{Sn}_3$  are shown in Table 4.

For stable structures, the elastic constants  $C_{ij}$  should satisfy the corresponding Born stability criterion [38]. For the cubic crystal system, the elastic constants should satisfy the following criteria:  $C_{11} - C_{12} > 0$ ,  $C_{11} + 2C_{12} > 0$  and  $C_{44} > 0$ . Observing Table 4, it can be found that the calculated elastic constants of the alloys satisfy the stability criterion, indicating that the Cu–Sn alloys are stable at 0 K. These results are consistent with the actual situation and correspond to the previously calculated mixing enthalpy results.

From the elastic constants, the corresponding bulk modulus  $B$ , shear modulus  $G$ , Young’s modulus  $E$ , and Poisson’s ratio  $\nu$  can be obtained using the Voigt–Reuss–Hill approximation [39]. The Voigt, Reuss, and Hill approximations of the elastic modulus are denoted by the subscripts  $V$ ,  $R$ , and  $H$ , respectively. For cubic structures, the modulus of elasticity can be defined as:

$$B_V = B_R = (C_{11} + 2C_{12})/3 \quad (12)$$

$$G_V = (C_{11} - C_{12} + 3C_{44})/5 \quad (13)$$

$$G_R = 5(C_{11} - C_{12})C_{44}/[4C_{44} + 3(C_{11} - C_{12})] \quad (14)$$

In the  $V$ - $R$ - $H$  model,  $B$  and  $G$  in the Hill model are obtained by taking the average of  $B$  or  $G$  in the Voigt and Reuss models,

$$B_H = \frac{1}{2}(B_V + B_R) \quad (15)$$

$$G_H = \frac{1}{2}(G_V + G_R) \quad (16)$$

Meanwhile, the relationship between Young's modulus  $E$  and Poisson's ratio  $\nu$  can be obtained,

$$E = \frac{9BG}{3B + G} \quad (17)$$

$$\nu = \frac{3B - 2G}{6B + 2G} \quad (18)$$

Calculated values of elastic parameters for Cu and Cu–Sn alloys ( $\text{Cu}_{31}\text{Sn}$ ,  $\text{Cu}_{30}\text{Sn}_2$ , and  $\text{Cu}_{29}\text{Sn}_3$ ) are presented in Table 5. In order to verify the reliability of the calculated results, the calculated values of the elastic parameters for copper in Table 4; Table 5 were compared with the previously reported experimental values [40–42] and theoretical values [43,44]. The elastic parameters obtained in this study are in better agreement with the reference values, indicating that the calculated parameters and method have high reliability and certain reference values.

**Table 4.** Elastic constants  $C_{ij}$  of Cu–Sn alloys. The present calculation results are compared with experimentally reported and other theoretical values.

Structure	Source	Elastic Constants of Crystals (GPa)								
		$C_{11}$	$C_{12}$	$C_{13}$	$C_{22}$	$C_{23}$	$C_{33}$	$C_{44}$	$C_{55}$	$C_{66}$
Cu	Present	184.5	116.7					77.1		
	Exp.at 4.2 K <sup>a</sup>	176.2	124.9					81.8		
	Exp.at RT <sup>b</sup>	170	122.5					75.8		
	Exp.at RT <sup>c</sup>	168.1	121.5					75.1		
	Cal. <sup>d</sup>	176	118.2					81.9		
	Cal. <sup>e</sup>	183.5	125.9					80.9		
$\text{Cu}_{31}\text{Sn}$	Present	182.98	109.79					78.13		
	Present (SBP)	182.93	109.73	109.69	183.01	109.71	182.80	78.13	78.13	78.13
$\text{Cu}_{30}\text{Sn}_2$	Present	158.44	130.77					61.33		
	Present (SBP)	158.27	129.82	128.96	159.97	129.74	156.39	61.34	61.35	61.35
$\text{Cu}_{29}\text{Sn}_3$	Present	160.51	107.29					75.63		
	Present (SBP)	160.69	106.89	106.40	161.68	106.97	159.88	75.62	75.62	75.62

<sup>a</sup> Experimental data reported in Ref. [40]. <sup>b</sup> Experimental data reported in Ref. [41]. <sup>c</sup> Experimental data reported in Ref. [42]. <sup>d</sup> Calculated data reported in Ref. [43]. <sup>e</sup> Calculated data reported in Ref. [44].

Figure 4a shows the changes in  $B_H$ ,  $G_H$ , and  $E$  of Cu,  $\text{Cu}_{31}\text{Sn}$ ,  $\text{Cu}_{30}\text{Sn}_2$ , and  $\text{Cu}_{29}\text{Sn}_3$  as the content of Sn increases. In general, the bulk modulus  $B_H$  is used to characterize the incompressibility of a material. The higher the  $B_H$  value, the less likely the material is to compress under external forces. The shear modulus  $G_H$  is defined as the ability of a material to resist shear deformation. If the shear modulus  $G_H$  is larger, it indicates that the directional bonding between atoms is more significant. The Young's modulus  $E$  is a physical quantity used to describe the stiffness of a material. As the Young's modulus  $E$  increases, the hardness of the material also increases.

**Table 5.** The calculated bulk modulus  $B_H$  (GPa), shear modulus  $G_H$  (GPa), Young's modulus  $E$  (GPa), Poisson's ratio  $\nu$ , Pugh's ratio  $G_H/B_H$ , Cauchy pressure  $C_{12}-C_{44}$ , dislocation strain energy  $W$ , and universal elastic anisotropy  $A^U$  for Cu–Sn alloys. The present calculation results are compared with experimentally reported and previously computed values.

Structure	Source	Modulus			$\nu$	$G_H/B_H$	$C_{12}-C_{44}$	$W/J\cdot m^{-1}$	$A^U$
		$B_H$ (GPa)	$G_H$ (GPa)	$E$ (GPa)					
Cu	Present	139.7	55.7	147.5	0.32	0.40	39.6	0.367	0.83
	Exp.at 4.2 K	142	51.5	137.8	0.34	0.36			1.80 [40]
	Exp.at RT	138.3	47.7	128.3	0.35	0.35			1.81 [41]
	Exp.at RT	137.0	47.1	126.7	0.35	0.34			1.84 [42]
	Cal.	137.4	54.0	143.3	0.33	0.39			1.42 [43]
	Cal.	145.1	53.5	142.9	0.34	0.37			1.40 [44]
Cu <sub>31</sub> Sn	Present	134.13	57.63	151.23	0.31	0.43	31.60	0.387	0.72
Cu <sub>30</sub> Sn <sub>2</sub>	Present	139.01	34.43	95.42	0.39	0.25	68.48	0.236	3.06
Cu <sub>29</sub> Sn <sub>3</sub>	Present	124.81	49.99	132.31	0.32	0.40	31.27	0.349	1.40

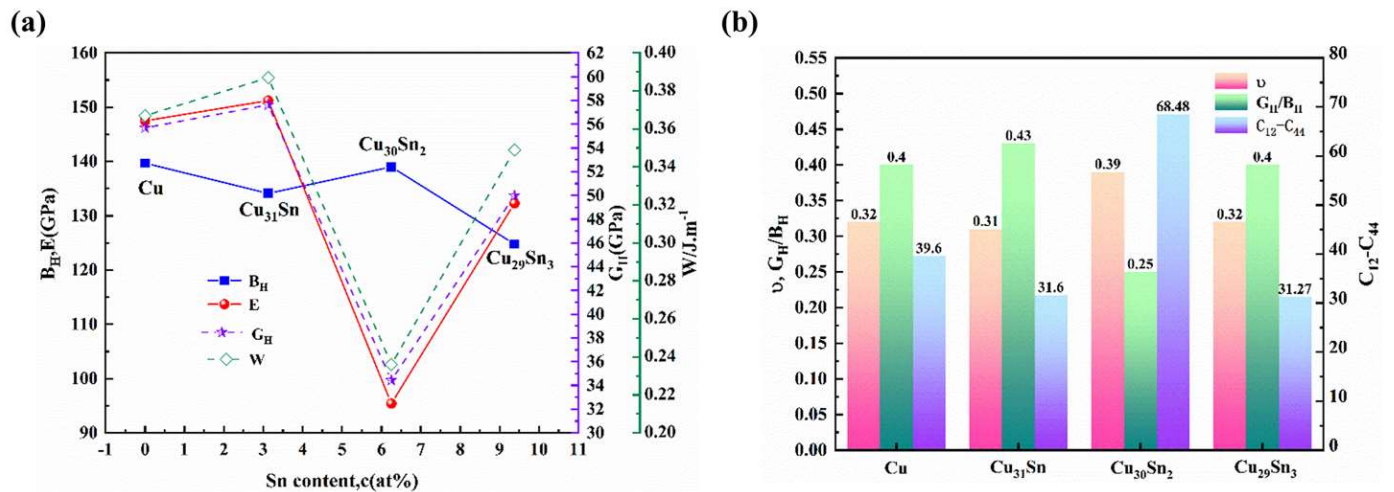


**Figure 4.** Variations in  $B_H$ ,  $G_H$ ,  $E$ , and  $W$  (a),  $\nu$ ,  $G_H/B_H$ , and  $C_{12}-C_{44}$  (b) for Cu–Sn alloys.

As can be seen from Figure 5a, the order of values for  $G_H$  and  $E$  is:  $Cu_{31}Sn > Cu > Cu_{29}Sn_3 > Cu_{30}Sn_2$ .  $Cu_{31}Sn$  has the highest  $G_H$  value (57.63 GPa) and the highest  $E$  value (151.23 GPa), while  $Cu_{30}Sn_2$  has the lowest  $G_H$  value (34.43 GPa) and the lowest  $E$  value (95.42 GPa), indicating that among these Cu–Sn alloys,  $Cu_{31}Sn$  has the most significant directional bonding, the strongest shear deformation resistance, and the highest hardness. On the contrary,  $Cu_{30}Sn_2$  has the weakest shear deformation resistance and the highest plasticity. In addition, in Cu–Sn alloys, the bulk modulus presents a “downward-upward-downward” trend with the increase of Sn content. Compared with pure Cu, an increase in Sn content will reduce its incompressibility.

The lattice distortion will occur when Sn is solidly dissolved into the Cu matrix. The elastic stress field caused by this deformation increases the crystal energy, which is defined as the strain energy of the dislocation [45],

$$W \approx Gb^2 \quad (19)$$

where  $G$  is the shear modulus and  $b$  is the Burgers vector. For fcc crystals,  $b^2 = 0.5a^2$ . The greater the dislocation strain energy, the poorer its plastic deformation ability, and the higher its tensile strength. The dislocation strain energy of Cu–Sn alloys is shown in Figure 4. With the increase of Sn content, the dislocation strain energy presents a trend of first increasing, then decreasing, and then increasing, indicating that its plastic deformation ability first decreases, then increases, and then decreases. This trend is the same as that

of shear modulus  $G$  and Young's modulus  $E$ , which can be explained by the dislocation motion theory.

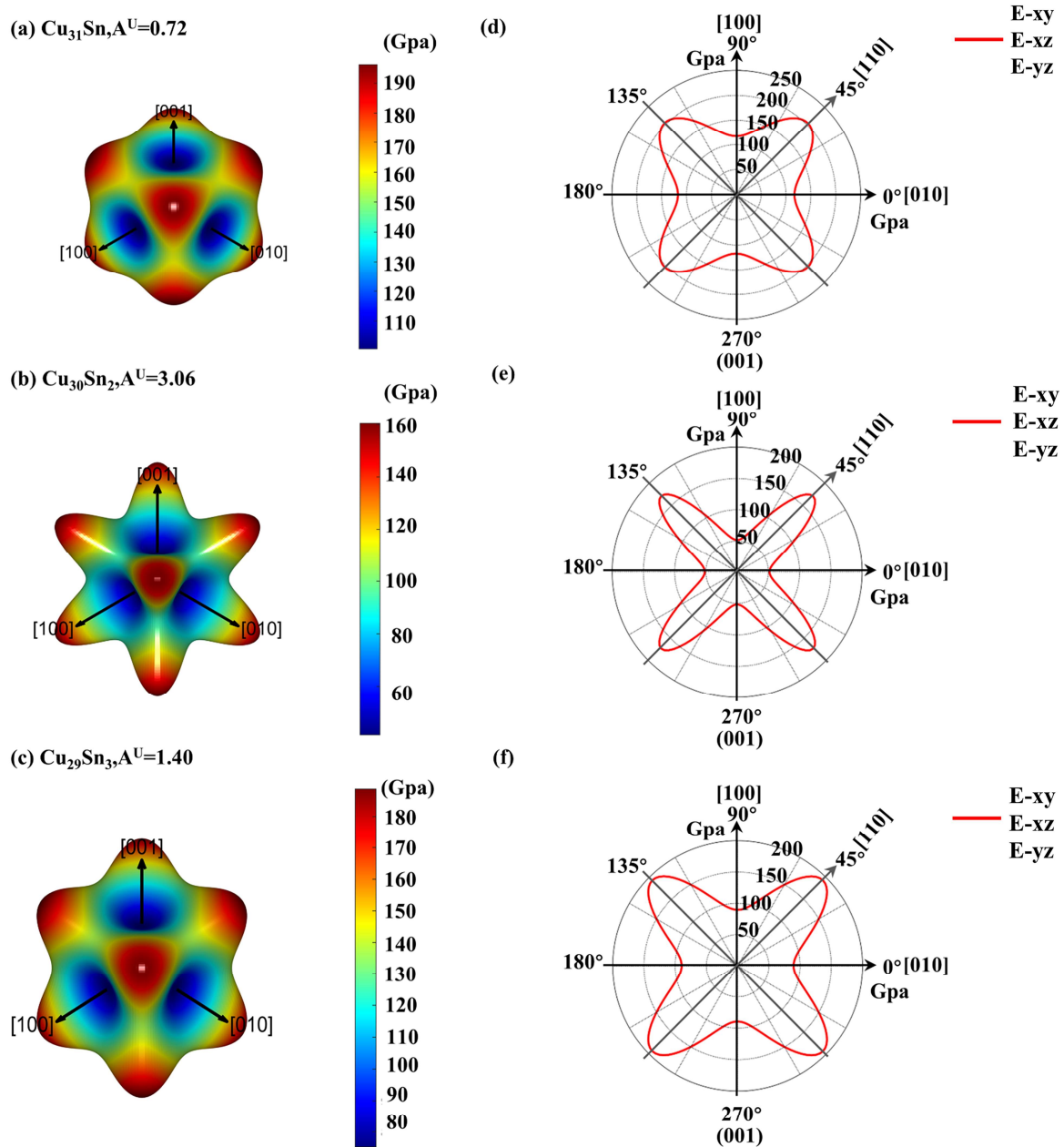


**Figure 5.** Three-dimensional surfaces (a–c) and planar projections (d–f) of the Young's modulus  $E$  for Cu–Sn alloys.

Elastic modulus and Poisson's ratio are important indicators that can reflect the mechanical properties of materials to a certain extent. However, to have a better understanding of their mechanical properties, in any service environment, it is also necessary to associate their bonding properties with toughness. Poisson's ratio  $\nu$ ,  $G_H/B_H$  [46], and Cauchy exact pressure on  $C_{12}-C_{44}$  [47] to evaluate the ductility trend of the material. According to Pettifor and Pugh criteria, ductile materials should meet:  $\nu > 0.26$ ,  $G_H/B_H < 0.57$ ,  $C_{12}-C_{44} > 0$ ; conversely, brittle materials:  $\nu < 0.26$ ,  $G_H/B_H > 0.57$ ,  $C_{12}-C_{44} < 0$ . From Table 5 and Figure 4b, these Cu–Sn alloys meet the toughness criteria and have ductility. With the increase of Sn content, the ductility presents a “downward-upward-downward” trend, with  $\text{Cu}_{30}\text{Sn}_2$  having the largest  $\nu$  (0.39),  $C_{12}-C_{44}$  maximum (68.48),  $G_H/B_H$  minimum (0.25), indicating that  $\text{Cu}_{30}\text{Sn}_2$  has the best ductility.

It is well known that elastic anisotropy is one of the causes that induce microcracking in materials [1]. Therefore, it is necessary to study its elastic anisotropy to evaluate the mechanical durability of Cu–Sn alloys. Among others, Ranganathan and Ostoja-Starzewski [48] improved the concept of the universal anisotropy index ( $A^U$ ) to study the degree of anisotropy in different directions of bonding between atoms in different crystal planes, which can be expressed as

$$A^U = 5 \frac{G_V}{G_R} + \frac{B_V}{B_R} - 6 \quad (20)$$

$A^U$  takes into account the contributions of both shear and bulk modulus, where the deviation of  $A^U$  from 0 determines the degree of crystal anisotropy, and as can be seen from Table 5,  $\text{Cu}_{30}\text{Sn}_2$  exhibits a higher degree of anisotropy compared to Cu,  $\text{Cu}_{31}\text{Sn}$ , and  $\text{Cu}_{29}\text{Sn}_3$ . Furthermore, this degree of anisotropy can be visually represented, as it is in Figure 5.

The Young's modulus  $E$  is not only color-coded in all directions by Elastic POST [49], but also its specific magnitude is shown in a two-dimensional plot. The Cu–Sn alloys examined in this study belong to the cubic crystal system, and the directional dependence of its Young's modulus can be obtained from the calculated flexibility constant [50], which can be expressed as

$$\frac{1}{E} = S_{11} - (2S_{11} - 2S_{12} - S_{44}) (l_1^2 l_2^2 + l_2^2 l_3^2 + l_3^2 l_1^2) \quad (21)$$

where  $E$  is the Young's modulus,  $S_{ij}$  is the elastic flexibility coefficient, and  $l_1, l_2$ , and  $l_3$  are the directional cosines.

Observing the three-dimensional diagram of Young's modulus anisotropy of Cu–Sn alloys in Figure 5a–c, the degree of elastic anisotropy of  $\text{Cu}_{30}\text{Sn}_2$  can be described in more detail using the ratio of directional elastic modulus in Planar Projection, Figure 5d–f. The greater the deviation of this ratio from 1, the higher the elastic anisotropy of the surface [48]. For cubic crystal systems, the directional elastic modulus satisfies the following conditions:  $[100] = [010] = [001] \neq [110]$ .  $E_{(100)}/E_{(110)}$  represents the directional Young's modulus elastic anisotropy in the (110) plane. According to Figure 5d–f, the Young's moduli of  $\text{Cu}_{31}\text{Sn}$ ,  $\text{Cu}_{30}\text{Sn}_2$ , and  $\text{Cu}_{29}\text{Sn}_3$  in the  $\langle 100 \rangle$  direction are 120 GPa, 50 GPa, and 85 GPa, respectively; the Young's moduli in the  $\langle 110 \rangle$  direction are 205 GPa, 175 GPa, and 190 GPa, respectively. The deviation between  $E_{(100)}/E_{(110)}$  and 1 for  $\text{Cu}_{30}\text{Sn}_2$  is the largest (0.714), followed by the deviation between  $E_{(100)}/E_{(110)}$  and 1 for  $\text{Cu}_{29}\text{Sn}_3$  (0.553), and the deviation between  $E_{(100)}/E_{(110)}$  and 1 for  $\text{Cu}_{31}\text{Sn}$  (0.415) is the smallest. This indicates that the Young's modulus anisotropy of Cu–Sn alloys satisfies the following requirements:  $\text{Cu}_{30}\text{Sn}_2 > \text{Cu}_{29}\text{Sn}_3 > \text{Cu}_{31}\text{Sn}$ , which is the same as the order of  $A^U$ .

### 3.5. Electronic Properties

The electronic structure can explain the source of mechanical properties at a microscopic level. To further grasp the phase stability and bonding characteristics of the Cu–Sn alloys, the relevant electronic properties of the solid solution were investigated based on structural optimization. Figure 6 shows the total density of states (TDOS) and the partial density of states (PDOS) of the Cu–Sn alloys in the energy range of  $-12$  eV to 6 eV. From Figure 6, it can be seen visually that the distribution of density of states and their trends are relatively similar for the Cu–Sn alloys. First, the TDOS below the Fermi energy level (0 eV) is contributed mainly by the Cu-3d states, with partial contributions from the Sn-5s and Sn-5p states, while the TDOS above the Fermi energy level mainly originates from the Sn-5s and Sn-5p states, while partly from the Cu-3p states. It is well known that the DOS values ( $N_{(\text{EF})}$ ) at the Fermi energy level are related to the phase stability, where the smaller the  $N_{(\text{EF})}$ , the more stable the corresponding phase is [51]. The  $N_{(\text{EF})}$  values of  $\text{Cu}_{31}\text{Sn}$ ,  $\text{Cu}_{30}\text{Sn}_2$ , and  $\text{Cu}_{29}\text{Sn}_3$  are 7.0843, 9.1978, and 8.6509 electrons/(eV·f.u.), respectively. The order of  $N_{(\text{EF})}$  values is  $\text{Cu}_{31}\text{Sn} < \text{Cu}_{29}\text{Sn}_3 < \text{Cu}_{30}\text{Sn}_2$ . As discussed earlier, the enthalpy of mixing

indicates that  $\text{Cu}_{31}\text{Sn}$  is the most stable. Second, all Cu–Sn alloys have non-zero TDOS values at the Fermi energy level, which indicates the metallic character of these Cu–Sn alloys. Thirdly, the peak values of the Cu-3d state undergo splitting at  $-4$  eV to  $-2$  eV. As the Sn content increases, the three peaks gradually change from uniform to non-uniform in  $\text{Cu}_{31}\text{Sn}$ ,  $\text{Cu}_{30}\text{Sn}_2$ , and  $\text{Cu}_{29}\text{Sn}_3$ , with a decrease at  $-4$  eV and an increase at  $-2$  eV. This is mainly attributed to the characteristics of the crystal structure and the symmetry of coordination, resulting in the crossing or overlapping of energy levels, which in turn affects the state and degree of peaks in DOS.

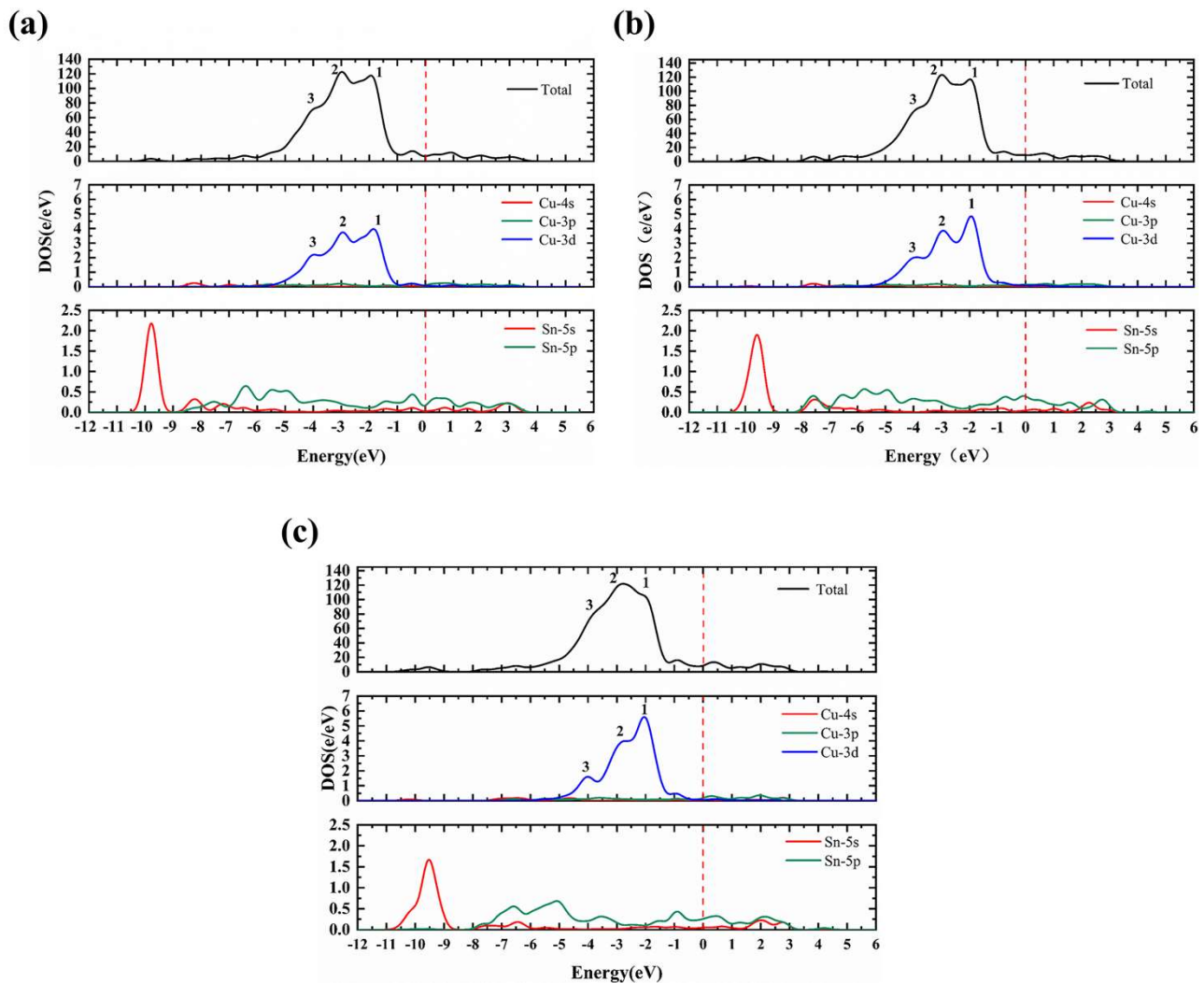


**Figure 6.** Total and partial electronic densities of states (TDOS and PDOS) near Fermi level of Cu–Sn alloys (a)  $\text{Cu}_{31}\text{Sn}$ , (b)  $\text{Cu}_{30}\text{Sn}_2$ , and (c)  $\text{Cu}_{29}\text{Sn}_3$ . The red dotted line indicates the Fermi level, and 1, 2, and 3 indicate the peak splitting of the Cu-3d state.

The differential charge density can directly characterize the nature of chemical bonding between different atoms and the electron gain and loss. Figure 7 shows the differential charge density diagram for Cu–Sn alloys in the range of  $-0.250$  to  $0.047$   $\text{e}/\text{\AA}^3$ , where the red region indicates the accumulation of electrons and the blue region indicates the depletion of electrons. As shown in Figure 7, in the Cu–Sn alloys, a large number of electrons gather between the Cu and Sn atoms, and the Cu atoms have a significant loss of charge in the outer layers, which can be clearly observed as a “sea of electrons” phenomenon, thus indicating the existence of metallic bonds [52]. As shown in Figure 7, the distribution of electron clouds around Cu atoms is in the shape of petal, with directionality. The petal distributions are closely related to the shapes of d orbitals [53]. Moreover, the electron cloud

is in the shape of petal, indicating that polarization is relatively severe, resulting in uneven distribution of electrons. It is speculated that there may be other bonds in the Cu matrix besides metal bonds. In addition, some electrons accumulate between Cu and adjacent Cu atoms, which indicates the presence of metallic bonds and Cu-Cu covalent bonds in Cu-Sn alloys. Among them, compared with Cu and adjacent Cu atoms, Cu and adjacent Sn atoms direction, the blue area around Cu is larger and dense, indicating a serious electron loss and the formation of stronger Cu-Sn covalent bonds. By the non-uniformity of the charge causes anisotropy in the relevant properties of the material (e.g., elastic properties). Observing Figure 7, it is found that the blue area around Cu in  $\text{Cu}_{30}\text{Sn}_2$  is large and dense compared to  $\text{Cu}_{31}\text{Sn}$  and  $\text{Cu}_{29}\text{Sn}_3$ , and the non-uniformity of the charge is more significant, thus its elastic anisotropy is the highest, reflecting the highest Young's modulus elastic anisotropy of  $\text{Cu}_{30}\text{Sn}_2$  discussed earlier. With the addition of the alloying element Sn, the distribution of electron clouds around the atoms changes subsequently, and the electron cloud of the Sn element has a red sphere shape, indicating the accumulation of electrons in the alloying element.

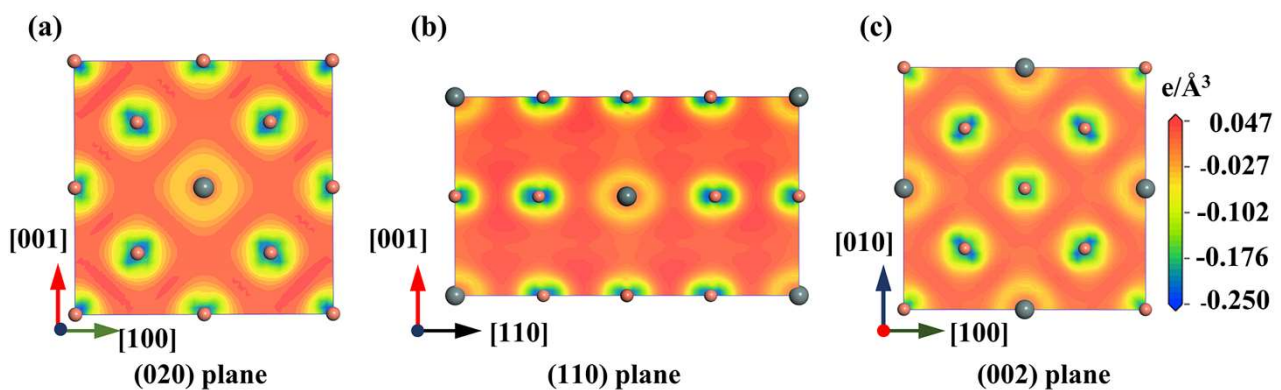


**Figure 7.** Charge density differences for Cu-Sn solid solutions (a)  $\text{Cu}_{31}\text{Sn}$ , (b)  $\text{Cu}_{30}\text{Sn}_2$  and (c)  $\text{Cu}_{29}\text{Sn}_3$ .

On the other hand, the atomic Mulliken charge (AMC) can adequately describe the charge transfer between Cu and Sn atoms. If the atom has a negative AMC, it indicates that this atom gains charge; otherwise, this atom loses charge. In  $\text{Cu}_{29}\text{Sn}_3$  and  $\text{Cu}_{31}\text{Sn}$ , most of the Cu atoms gain charge from Sn atoms or other Cu atoms, and some lose charge. In  $\text{Cu}_{30}\text{Sn}_2$ , most of the Cu atoms gain charge from Sn atoms or other Cu atoms, and a few have no gain or loss of electrons. Bond population (BP) and the bond length  $L$  are also important parameters to assess the bonding properties. In general, the shorter the bond length  $L$  and the larger bond population (BP), the stronger the bond, and a bond with a BP value of zero is a perfect ionic bond; otherwise, it is a covalent bond. A larger absolute BP value indicates a stronger covalent bond. Positive and negative BP values indicate bonding interactions and antibonding interactions in the bond, respectively [54,55]. As shown in Table 6, the BP values of Cu-Sn bonds and Cu-Cu bonds in these Cu-Sn alloys are much larger than zero, thus indicating the presence of Cu-Sn covalent bonds and Cu-Cu covalent bonds. Furthermore, it can be found that Sn-Sn bonds do not exist in these Cu-Sn alloys. Therefore, Sn atoms are prone to displacement and will first form vacancies at Sn sites [47]. It was shown that bond population (BP) is also an important indicator of the mechanical properties of the material. In general, the phase stability, shear modulus and hardness of Cu-Sn alloys are positively correlated with the strength of the covalent bond, and this relationship can be obtained by bond population (BP), and the stronger the covalent bond, the larger bond population (BP). The strong phase stability, shear modulus and hardness of  $\text{Cu}_{31}\text{Sn}$  obtained in this study can be attributed to the formation of a stronger Cu-Cu covalent bond.

**Table 6.** Atomic Mulliken charge (AMC), bond population (BP) analysis and mean bond length (Å) for Cu–Sn alloys. The numbers in brackets for the atom represent the number of Cu or Sn ions, whereas the number in brackets for the bond represents the number of Cu–Cu and Cu–Sn bonds.

Species	Atom	Charge Number				AMC	Bond	BP	Length (Å)
		<i>s</i>	<i>p</i>	<i>d</i>	Total				
Cu <sub>31</sub> Sn	Cu(1)	0.51	0.77	9.72	11.01	−0.01	Cu–Cu(12)	0.27	2.50443
	Cu(12)	0.51	0.78	9.72	11.01	−0.01	Cu–Cu(48)	0.23	2.5588
	Cu(3)	0.51	0.81	9.72	11.03	−0.03	Cu–Cu(12)	0.2	2.57028
	Cu(12)	0.53	0.81	9.73	11.06	−0.06	Cu–Cu(24)	0.21	2.57028
	Cu(3)	0.51	0.74	9.73	10.98	0.02	Cu–Cu(24)	0.19	2.59082
	Sn(1)	0.65	2.42	0	3.08	0.92	Cu–Cu(24)	0.21	2.59218
							Cu–Cu(12)	0.19	2.61121
							Cu–Cu(24)	0.16	2.67706
						Cu–Sn(12)	0.17	2.67706	
Cu <sub>30</sub> Sn <sub>2</sub>	Cu(24)	0.53	0.82	9.73	11.07	−0.07	Cu–Cu(8)	0.26	2.54638
	Cu(6)	0.51	0.77	9.73	11	0	Cu–Cu(16)	0.26	2.54639
	Sn(2)	0.71	2.42	0	3.13	0.87	Cu–Cu(44)	0.26	2.54828
							Cu–Cu(26)	0.2	2.61677
							Cu–Cu(22)	0.2	2.61678
							Cu–Sn(8)	0.18	2.68531
							Cu–Cu(45)	0.16	2.68531
							Cu–Cu(12)	0.18	2.68532
							Cu–Cu(4)	0.16	2.68532
							Cu–Sn(3)	0.18	2.68533
Cu <sub>29</sub> Sn <sub>3</sub>	Cu(12)	0.54	0.85	9.74	11.13	−0.13	Cu–Cu(12)	0.24	2.56039
	Cu(10)	0.52	0.82	9.73	11.07	−0.07	Cu–Cu(24)	0.26	2.56039
	Cu(3)	0.5	0.71	9.74	10.96	0.04	Cu–Cu(12)	0.23	2.62491
	Cu(1)	0.5	0.66	9.75	10.92	0.08	Cu–Cu(59)	0.21	2.64287
	Sn(3)	0.79	2.46	0	3.25	0.75	Cu–Cu(48)	0.19	2.67471
							Cu–Sn(12)	0.14	2.72284

### 3.6. Debye Temperature

The Debye temperature ( $\theta_D$ ) is an important parameter of crystalline materials. On the one hand, it can reflect the thermal properties of the material, and on the other hand, it can be used as a link between the thermal and mechanical properties of the material. At low temperatures, the acoustic vibration is the only factor that triggers the vibration excitation, so at low temperatures, the Debye temperature calculated by the elastic constant is equivalent to the Debye temperature determined by the specific heat measurement. Thus, it can be calculated by the following equation [56,57],

$$\theta_D = \frac{h}{k} \left[ \frac{3n}{4\pi} \left( \frac{N_A \rho}{M} \right) \right]^{\frac{1}{3}} v_m \quad (22)$$

where  $h$ ,  $k$ , and  $N_A$  are Planck's constant, Boltzmann's constant, and Avogadro's constant, respectively,  $n$  is the total number of atoms per unit cell,  $\rho$  is the density,  $M$  is the molecular weight, and  $v_m$  is the average speed of sound, which can be defined as [57,58],

$$v_m = \left[ \frac{1}{3} \left( \frac{2}{v_t^3} + \frac{1}{v_l^3} \right) \right]^{-\frac{1}{3}} \quad (23)$$

where  $v_l$  and  $v_t$  are the longitudinal and transverse sound velocities, respectively, and can be obtained from the shear modulus  $G$ , the bulk modulus  $B$ , and the density  $\rho$ , which are related as follows,

$$v_l = \left( \frac{B + \frac{4}{3}G}{\rho} \right)^{\frac{1}{2}} \quad (24)$$

$$v_t = \left( \frac{G}{\rho} \right)^{\frac{1}{2}} \quad (25)$$

The calculated Debye temperatures, sound velocities and densities of pure Cu, and Cu–Sn alloys are shown in Table 7, which shows that the calculated sound velocities and Debye temperatures of Cu are in good agreement with the experimental values and previous calculations by scholars. In general, the higher the Debye temperature, the higher the melting point of the corresponding crystal and the stronger the covalent bond, the more stable the structure. As shown in Table 7 and Figure 8, among the Cu–Sn alloys, the Debye temperature of Cu<sub>31</sub>Sn is the highest, the corresponding covalent bond strength is the strongest, and the stability is the best, which is exactly in line with the results discussed in Table 2 and Figure 4a.

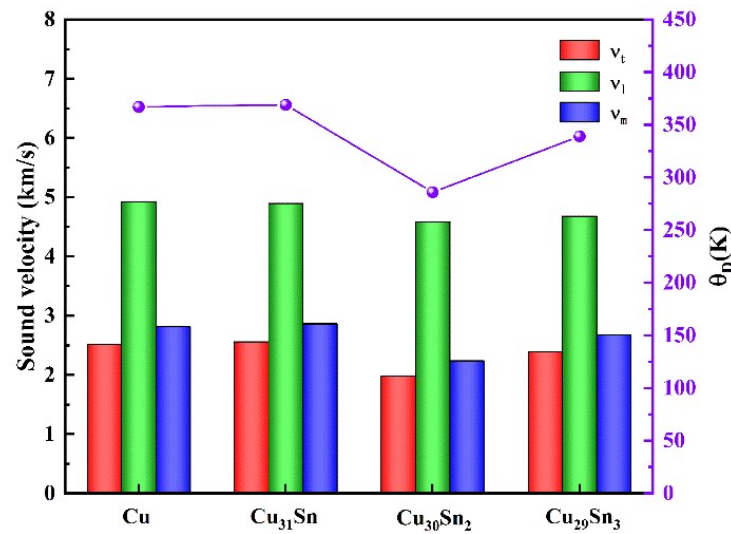


**Figure 8.** Variations in the sound velocity and Debye temperature for Cu–Sn alloys.

In addition, the lattice thermal conductivity  $\kappa_{ph}$  is also one of the most fundamental physical properties of the material, which characterizes the thermal conductivity of the material and is of great significance for exploring the application of the material at high temperatures. In general, we consider the minimum value of the lattice thermal conductivity  $k_{min}$  [59], which is related by the equation,

$$k_{min} = \frac{k_B}{2.48} n^{\frac{2}{3}} (2v_t + v_l) \quad (26)$$

where  $k_B$  is the Boltzmann constant,  $n$  is the number of atoms per unit volume, and  $v_l$  and  $v_t$  are the longitudinal and transverse velocities of sound, respectively.

Melting point is also an important parameter of the material and is currently a hot issue of research, playing a crucial role in predicting new intermetallic compounds for high-temperature applications. It can be obtained by the following empirical equation [60],

$$T_m = 354 + 4.5 \frac{2C_{11} + C_{33}}{3} \quad (27)$$

In addition to the speed of sound ( $v_l$ ,  $v_t$ ,  $v_m$ ) and Debye temperature  $\theta_D$ , the density  $\rho$ , the minimum value of lattice thermal conductivity  $k_{min}$ , and the melting point  $T_m$  of the Cu–Sn alloys are included in Table 7. It can be found that the minimum value of lattice thermal conductivity and melting point of Cu–Sn alloys follow the following pattern: Cu<sub>31</sub>Sn > Cu<sub>29</sub>Sn<sub>3</sub> > Cu<sub>30</sub>Sn<sub>2</sub>. The above calculation results indicate that Cu–Sn alloys are good thermally conductive materials, and it is tentatively predicted that the thermal conductivity of Cu–Sn alloy is relatively good when the Sn content is low. However, there

are few reports on the experimental Debye temperature and other thermal properties of Cu–Sn alloys. Therefore, it is hoped that the results of the present calculations can provide a reference value for subsequent studies of Cu–Sn alloys.

**Table 7.** The calculated and experimental results of density ( $\rho$ ), transverse, longitudinal, average sound velocity ( $v_t, v_l, v_m$  in m/s), Debye temperatures ( $\theta_D$ , K), the minimum thermal conductivity ( $k_{min}$  in  $\text{Wm}^{-1}\text{K}^{-1}$ ) and melting point ( $T_m$  in K) of Cu–Sn alloys.

Structure	Source	$\rho$	$v_t$	$v_l$	$v_m$	$\theta_D$	$\kappa_{min}$	$T_m$	Refs.
Cu	Present	8.828	2512	4923	2815	367	1.06	1184	
	Exp.	8.937						1353	[61]
	Exp.					343			[62]
	Cal.	9.353	2639	5209	2958	391	1.16	1330	[63]
	Cal.	8.930	2277	4723	2560	335			[47]
Cu <sub>31</sub> Sn	Present	8.815	2557	4892	2861	369	1.19	1177	
Cu <sub>30</sub> Sn <sub>2</sub>	Present	8.787	1980	4587	2237	286	0.88	1066	
Cu <sub>29</sub> Sn <sub>3</sub>	Present	8.754	2390	4677	2678	339	0.96	1077	

#### 4. Conclusions

The lattice constants, phase stability, solution strengthening, elastic properties, electronic properties, and Debye temperature of Cu–Sn alloys with different Sn contents (Cu<sub>31</sub>Sn, Cu<sub>30</sub>Sn<sub>2</sub>, Cu<sub>29</sub>Sn<sub>3</sub>) were studied by first principles. The relevant conclusions are as follows.

The calculated lattice constants are proportional to the solute concentration, consistent with the Vegard's law, and have a linear relationship across the entire Cu–Sn solid solution region; the Sn atoms of 3.125 at%, 6.25 at%, and 9.375 at% can be solidly dissolved in the Cu matrix. The negative mixing enthalpy of Cu<sub>31</sub>Sn (3.125 at%) is the largest, indicating that its chemical bond is the strongest and its structure is the most stable. In the aspect of solution strengthening, the mismatch strain parameter is introduced to quantify the effect of solution strengthening. The calculated values can be used to predict the solution strengthening effect of Cu-based solid solutions, and are of great significance for developing copper alloys with ultra-high yield strength.

In Cu–Sn alloys, Cu<sub>30</sub>Sn<sub>2</sub> has the smallest shear modulus and Young's modulus. Its variation trend is the same as that of dislocation strain energy (Cu<sub>30</sub>Sn<sub>2</sub> has a minimum dislocation strain energy of  $0.236 \text{ Jm}^{-1}$ ), indicating that when the Sn content is 6.25 at%, the plasticity of Cu–Sn alloys is the largest. In addition, Cu<sub>30</sub>Sn<sub>2</sub> has the highest Young's modulus and elastic anisotropy.

The electronic structure and bonding properties of the Cu–Sn alloys have been calculated, and their relationship with the stability and mechanical properties of the alloys is analyzed and discussed. Three types of bonding existed in Cu–Sn alloys: Cu–Cu covalent bonds, Cu–Cu metallic bonds, and Cu–Sn covalent bonds, of which Cu<sub>31</sub>Sn had the best stability and the highest shear modulus, which depended to a certain extent on the fact that it had stronger Cu–Cu covalent bonds.

The Debye temperature of the Cu–Sn alloys, the minimum lattice thermal conductivity, and the melting point all decrease sequentially along the order of Cu<sub>31</sub>Sn, Cu<sub>29</sub>Sn<sub>3</sub>, and Cu<sub>30</sub>Sn<sub>2</sub>. This indicates that Cu–Sn alloys are good thermal conductivity materials. Additionally, it is tentatively predicted that the thermal conductivity of Cu–Sn alloy is relatively good when Sn content is low.

**Author Contributions:** L.Z., Y.L., X.W. and R.Z. designed most of the experiments, L.Z. analyzed the results and wrote this manuscript, Y.L. helped analyze the experiment data and gave some constructive suggestions about how to write this manuscript. L.Z., L.X., Q.W. and Z.L. performed most experiments. B.X. provided financial support. All authors have read and agreed to the published version of the manuscript.

**Funding:** This work was financially supported by the National Natural Science Foundation of China (No.52205373).

**Data Availability Statement:** Not applicable.

**Acknowledgments:** The authors gratefully acknowledge the National Natural Science Foundation of China (No.52205373) for the financial support of this research work.

**Conflicts of Interest:** The authors declare no conflict of interest.

## Appendix A

### Appendix A.1 Modeling Method:Script

```
1:
use strict;use Getopt::Long;
use MaterialsScript qw(:all);
my $disorderedStructure = $Documents{"Cu31Sn.xsd"};
my $results = Tools->Disorder->StatisticalDisorder->GenerateSuperCells
($disorderedStructure,2,2,2);
my $table = $results->StudyTable;
print "Number of disorder configurations generated:". $results->NumIrreducibleConfigurations.
"\n";
```

```
2:
use strict;
use Getopt::Long;
use MaterialsScript qw(:all);
my $disorderedStructure = $Documents{"Cu30Sn2.xsd"};
my $results = Tools->Disorder->StatisticalDisorder->GenerateSuperCells
($disorderedStructure,2,2,2);
my $table = $results->StudyTable;
print "Number of disorder configurations generated:". $results->NumIrreducibleConfigurations.
"\n";
```

```
3:
use strict;
use Getopt::Long;
use MaterialsScript qw(:all);
my $disorderedStructure = $Documents{"Cu29Sn3.xsd"};
my $results = Tools->Disorder->StatisticalDisorder->GenerateSuperCells
($disorderedStructure,2,2,2);
my $table = $results->StudyTable;
print "Number of disorder configurations generated:". $results->NumIrreducibleConfigurations.
"\n";
```

### Note:

This script references the content of the following web site: <https://zhuanlan.zhihu.com/p/50322042>.

Table A1. Structures.

Structures		Weighting	Configuration	E (eV/atom)
Cu <sub>31</sub> Sn	1	32	baaaaaaaaaaaaaaaaaaaaaaaaaaaa	-45,867.723
Cu <sub>30</sub> Sn <sub>2</sub>	1	192	baaaaaaaaaabaaaaaaaaaaaaaaaa	-44,485.574
	2	192	baaaaaabaaaaaaaaaaaaaaaaaaaa	-44,484.631
	3	16	baaaaaabaaaaaaaaaaaaaaaaaaaa	-44,485.663
	4	48	baabaaaaaaaaaaaaaaaaaaaaaaaa	-44,485.603
	5	48	bbaaaaaaaaaaaaaaaaaaaaaaaaaaaa	-44,485.427
Cu <sub>29</sub> Sn <sub>3</sub>	1	256	baaaaaaaaaabaaaaabaaaaaaaaaaa	-43,103.560
	2	768	baaaaaabaaaaaaaaabaaaaaaaaaaaa	-43,102.542
	3	768	baaaaaabaaaaaaaaabaaaaaaaaaaaa	-43,101.536
	4	256	baaaaaabaaaaaaaaabaaaaaaaaaaaa	-43,100.554
	5	384	baaaaaabaaaaaaaaaaaaaaaaaaaaaa	-43,102.624
	6	768	baabaaaaaaaaabaaaaaaaaaaaaaaaa	-43,102.558
	7	192	baabaaaaaaaaabaaaaaaaaaaaaaaaa	-43,103.594
	8	192	baabaaaabaaaaaaaaaaaaaaaaaaaaa	-43,101.576
	9	32	baababaaaaaaaaaaaaaaaaaaaaaaaa	-43,103.623
	10	384	bbaaaaaaaaaaaaaaaaabaaaaaaaaaa	-43,102.360
	11	384	bbaaaaaaaaabaaaaaaaaaaaaaaaaaaa	-43,103.366
	12	384	bbaaaaaaaaabaaaaaaaaaaaaaaaaaaa	-43,101.419
	13	96	bbaaaabaaaaaaaaaaaaaaaaaaaaaaa	-43,103.483
	14	96	bbbaaaaaaaaaaaaaaaaaaaaaaaaaaaa	-43,103.230

Appendix A.2

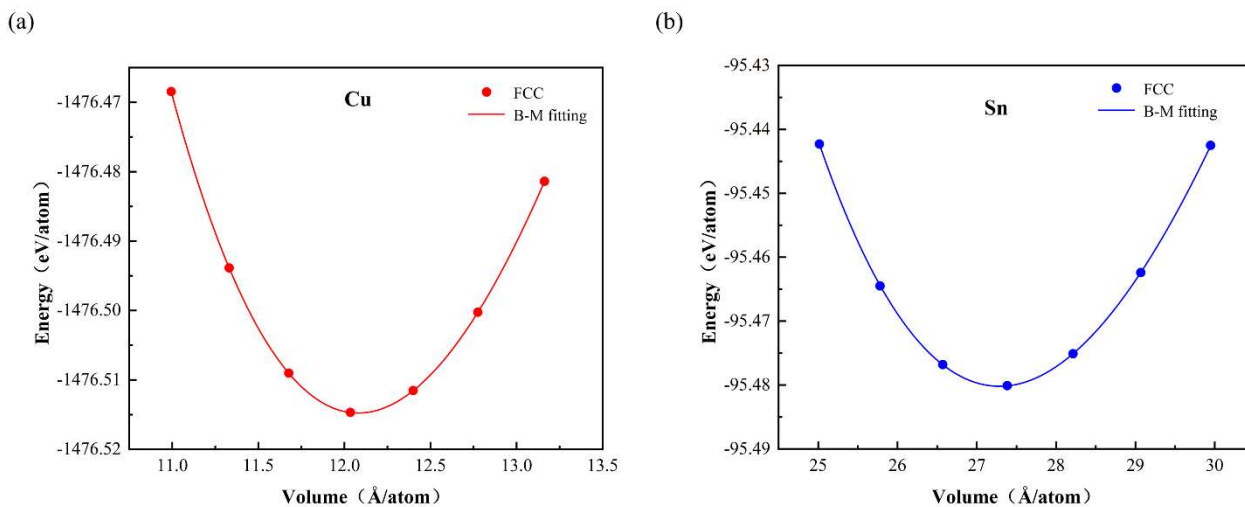


Figure A1. E-V fitting curves of pure elements (a) Cu, (b) Sn.

Appendix A.3

Table A2. Equilibrium volume  $V_0$  ( $\text{\AA}^3/\text{atom}$ ), bulk modulus  $B_0$  (GPa), first-order derivative of bulk modulus with respect to pressure  $B_0'$  and static energy  $E_0$  (eV/atom) of Cu and Sn.

Element	Pure			
	$V_0$ ( $\text{\AA}^3/\text{atom}$ )	$B_0$ (GPa)	$B_0'$	$E_0$ (eV/atom)
Cu	12.04	128.16	4.33	-1476.515
Sn	27.29	54.47	4.40	-95.480

## Appendix A.4

**Table A3.** Volume  $V$  ( $\text{\AA}^3/\text{atom}$ ) and total energy  $E$  (eV/atom) of the Cu–Sn alloys.

Structure	$V$ ( $\text{\AA}^3/\text{atom}$ )	$E$ (eV/atom)
Cu <sub>31</sub> Sn	393.47	−45,868.47
Cu <sub>30</sub> Sn <sub>2</sub>	405.02	−44,487.20
Cu <sub>29</sub> Sn <sub>3</sub>	417.17	−43,105.81

## References

- Yang, L.; Kang, H. Measurements of mechanical properties of  $\alpha$ -phase in Cu–Sn alloys by using instrumented nanoindentation. *J. Mater. Res.* **2012**, *27*, 192–196.
- Sun, J.; Ming, T.Y. Electrochemical behaviors and electrodeposition of Single-Phase Cu–Sn Alloy coating in [BMIM]Cl. *Electrochim. Acta* **2018**, *297*, 87–93.
- Liu, Y.; Wang, L. Electro-deposition preparation of self-standing Cu–Sn alloy anode electrode for lithium ion battery. *J. Alloys Compd.* **2019**, *775*, 818–825. [[CrossRef](#)]
- Singh, J.B.; Cai, W. Dry sliding of Cu–15 wt%Ni–8 wt%Sn bronze: Wear behaviour and microstructures. *Wear* **2007**, *263*, 830–841. [[CrossRef](#)]
- Zhu, S.Q.; Ringer, S.P. On the role of twinning and stacking faults on the crystal plasticity and grain refinement in magnesium alloys. *Acta Mater.* **2017**, *144*, 365–375. [[CrossRef](#)]
- Wen, Y.F.; Sun, J. Elastic stability of face-centered cubic Fe–Cu random solid solution alloys based on special quasirandom structure model. *Chin. J. Nonferrous Met.* **2012**, *22*, 2522–2528.
- Wei, Z.; Liu, L. Structural, electronic and thermo-elastic properties of Cu<sub>6</sub>Sn<sub>5</sub> and Cu<sub>5</sub>Zn<sub>8</sub> intermetallic compounds: First-principles investigation. *Intermetallics* **2010**, *18*, 922–928.
- An, R.; Wang, C. Determination of the Elastic Properties of Cu<sub>3</sub>Sn Through First-Principles Calculations. *J. Electron. Mater.* **2008**, *37*, 477–482.
- Davis, J.R. *ASM Specialty Handbook: Copper and Copper Alloys*; ASM International: Almere, The Netherlands, 2001.
- Scudino, S.; Unterdoerfer, C. Additive manufacturing of Cu–10Sn bronze. *Mater. Lett.* **2015**, *156*, 202–204. [[CrossRef](#)]
- Ping, H.; Xiao, F.R. Influence of hot pressing temperature on the microstructure and mechanical properties of 75% Cu–25% Sn alloy. *Mater. Des.* **2014**, *53*, 38–42.
- Payne, M.C.; Teter, M.P. Iterative minimization techniques for ab initio total-energy calculations: Molecular dynamics and conjugate gradients. *Rev. Mod. Phys.* **1992**, *64*, 1045. [[CrossRef](#)]
- Ming, X.; Wang, X.L. First-principles study of pressure-induced magnetic transition in siderite FeCO<sub>3</sub>. *J. Alloys Compd.* **2011**, *510*, L1–L4. [[CrossRef](#)]
- Varadachari, C.; Ghosh, A. Theoretical Derivations of a Direct Band Gap Semiconductor of SiC Doped with Ge. *J. Electron. Mater.* **2014**, *44*, 167–176.
- Ullrich, C.A.; Kohn, W. Degeneracy in Density Functional Theory: Topology in the v and n Spaces. *Phys. Rev. Lett.* **2002**, *89*, 156401. [[CrossRef](#)] [[PubMed](#)]
- Perdew, J.P.; Burke, K. Generalized Gradient Approximation Made Simple. *Phys. Rev. Lett.* **1996**, *77*, 3865. [[CrossRef](#)] [[PubMed](#)]
- Head, J.D.; Zerner, M.C. A Broyden–Fletcher–Goldfarb–Shanno optimization procedure for molecular geometries. *Chem. Phys. Lett.* **1985**, *122*, 264–270. [[CrossRef](#)]
- Liu, Y.; Liu, T. Research progress on intermetallic compounds and solid solutions of Mg alloys based on first-principles calculation. *Chongqing Daxue Xuebao/J. Chongqing Univ.* **2018**, *41*, 30–44.
- Straumanis, M.E.; Yu, L.S. Lattice parameters, densities, expansion coefficients and perfection of structure of Cu and of Cu–In  $\alpha$  phase. *Acta Crystallogr.* **2014**, *25*, 676–682. [[CrossRef](#)]
- Uesugi, T.; Higashi, K. First-principles studies on lattice constants and local lattice distortions in solid solution aluminum alloys. *Comput. Mater. Sci.* **2013**, *67*, 1–10. [[CrossRef](#)]
- Sidot, E.; Kahn-Harari, A. The lattice parameter of  $\alpha$ -bronzes as a function of solute content: Application to archaeological materials. *Mater. Sci. Eng. A* **2005**, *393*, 147–156. [[CrossRef](#)]
- Liu, T.; Chong, X.Y. Changes of alloying elements on elasticity and solid solution strengthening of  $\alpha$ -Ti alloys: A comprehensive high-throughput first-principles calculations. *Rare Met.* **2022**, *41*, 2719–2731. [[CrossRef](#)]
- Mxw, A.; Hong, Z.B. Solid-solution strengthening effects in binary Ni-based alloys evaluated by high-throughput calculations. *Mater. Des.* **2020**, *198*, 109359.
- Petrman, V.; Houska, J. Trends in formation energies and elastic moduli of ternary and quaternary transition metal nitrides. *J. Mater. Sci.* **2013**, *48*, 7642–7651. [[CrossRef](#)]
- Cottrell, A. Effect of solute atoms on the behavior of dislocations. In *Report of a Conference on Strength of Solids*; The Physical Society London: London, UK, 1948; pp. 30–36.
- Fleischer, R.L. Substitutional solution hardening. *Acta Metall.* **1963**, *11*, 203–209. [[CrossRef](#)]
- Suzuki, H. Segregation of Solute Atoms to Stacking Faults. *J. Phys. Soc. Jpn.* **1962**, *17*, 322–325. [[CrossRef](#)]

28. Cottrell, A.H.; Hunter, S.C. CXI. Electrical interaction of a dislocation and a solute atom. *Philos. Mag.* **1953**, *44*, 1064–1067. [[CrossRef](#)]
29. Friedel, J. Hardness of a Crystal Containing Uniformly Distributed Impurities or Precipitates. *Dislocations* **1964**, *20*, 368–384.
30. Uesugi, T.; Takigawa, Y. Deformation Mechanism of Nanocrystalline Al-Fe Alloys by Analysis from Ab-Initio Calculations. *Mater. Sci. Forum* **2006**, *503–504*, 209–214. [[CrossRef](#)]
31. Sms, A.; Kyk, A. Effects of Sn content and hot deformation on microstructure and mechanical properties of binary high Sn content Cu–Sn alloys. *Mater. Sci. Eng. A* **2020**, *796*, 140054.
32. Shi, J.G.; Liu, P. Selective Laser Melting Experiment of Cu<sub>10</sub>Sn Alloy. *Ind. Technol. Innov.* **2018**, *5*, 7–11.
33. Mao, Z.; Zhang, D.Z. Processing optimisation, mechanical properties and microstructural evolution during selective laser melting of Cu-15Sn high-tin bronze. *Mater. Sci. Eng. A* **2018**, *721*, 125–134. [[CrossRef](#)]
34. Page, Y.L.; Saxe, P. Symmetry-General Least-Squares Extraction of Elastic Data for Strained Materials From ab Initio Calculations of Stress. *Phys. Rev. B* **2002**, *65*, 104104. [[CrossRef](#)]
35. Jy, A.; Po, A. First-Principles Study of the Effect of Aluminum Content on the Elastic Properties of Cu-Al Alloys. *Mater. Today Commun.* **2022**, *31*, 103399.
36. Browaeys, J.T.; Chevrot, S. Decomposition of the elastic tensor and geophysical applications. *Geophys. J. R. Astron. Soc.* **2010**, *159*, 667–678. [[CrossRef](#)]
37. Moakher, M.; Norris, A.N. The Closest Elastic Tensor of Arbitrary Symmetry to an Elasticity Tensor of Lower Symmetry. *J. Elast.* **2006**, *85*, 215–263. [[CrossRef](#)]
38. Waller, I. Dynamical Theory of Crystal Lattices by M. Born and K. Huang. *Acta Crystallogr.* **1956**, *9*, 837–838. [[CrossRef](#)]
39. Chung, D.H.; Buessem, W.R. The Voigt-Reuss-Hill Approximation and Elastic Moduli of Polycrystalline MgO, CaF<sub>2</sub>, β-ZnS, ZnSe, and CdTe. *J. Appl. Phys.* **1967**, *38*, 2535–2540. [[CrossRef](#)]
40. Overton, W.C.; Gaffney, J. Temperature Variation of the Elastic Constants of Cubic Elements. I. Copper. *Phys. Rev.* **1955**, *98*, 969–977. [[CrossRef](#)]
41. Chang, Y.A.; Himmel, L. Temperature Dependence of the Elastic Constants of Cu, Ag, and Au above Room Temperature. *J. Appl. Phys.* **1966**, *37*, 3567–3572. [[CrossRef](#)]
42. Schmunk, R.E.; Smith, C.S. Elastic constants of copper-nickel alloys. *Acta Metall.* **1960**, *8*, 396–401. [[CrossRef](#)]
43. Cheng, L.; Shuai, Z. Insights into structural and thermodynamic properties of the intermetallic compound in ternary Mg–Zn–Cu alloy under high pressure and high temperature. *J. Alloys Compd.* **2014**, *597*, 119–123. [[CrossRef](#)]
44. Zhou, W.; Liu, L. Structural, Elastic, and Electronic Properties of Al-Cu Intermetallics from First-Principles Calculations. *J. Electron. Mater.* **2009**, *38*, 356–364. [[CrossRef](#)]
45. Li, F.; Chen, Y. First-Principles Calculations on the Enhancing Effect of Zr on the Mechanical and Thermodynamic Properties of Ir–Rh Alloys. *Trans. Indian Inst. Met.* **2023**, *76*, 1809–1817. [[CrossRef](#)]
46. Pugh, S.F. XCII. Relations between the elastic moduli and the plastic properties of polycrystalline pure metals. *Philos. Mag.* **2009**, *45*, 823–843. [[CrossRef](#)]
47. Qu, D.; Li, C. Structural, electronic, and elastic properties of orthorhombic, hexagonal, and cubic Cu<sub>3</sub>Sn intermetallic compounds in Sn–Cu lead-free solder. *J. Phys. Chem. Solids* **2019**, *138*, 109253. [[CrossRef](#)]
48. Ranganathan, S.I.; Ostoja-Starzewski, M. Universal Elastic Anisotropy Index. *Phys. Rev. Lett.* **2008**, *101*, 055504. [[CrossRef](#)] [[PubMed](#)]
49. Liao, M.; Yong, L. Alloying effect on phase stability, elastic and thermodynamic properties of Nb-Ti-V-Zr high entropy alloy. *Intermetallics* **2018**, *101*, 152–164. [[CrossRef](#)]
50. Shuvalov, L.A. *Electrical Properties of Crystals*; Springer: Berlin/Heidelberg, Germany, 1988.
51. Ma, L.; Duan, Y. Phase stability, anisotropic elastic properties and electronic structures of C15-type Laves phases ZrM<sub>2</sub> (M = Cr, Mo and W) from first-principles calculations. *Philos. Mag.* **2017**, *97*, 2406–2424. [[CrossRef](#)]
52. Zhu, Y.D.; Yan, M.F. First-principles investigation of structural, mechanical and electronic properties for Cu–Ti intermetallics. *Comput. Mater. Sci.* **2016**, *123*, 70–78. [[CrossRef](#)]
53. Wei, Y.A.; Yz, A. Investigation on elastic properties and electronic structure of dilute Ir-based alloys by first-principles calculations. *J. Alloys Compd.* **2021**, *850*, 156548.
54. Segall, M.; Shah, R. Population analysis of plane-wave electronic structure calculations of bulk materials. *Phys. Rev. B Condens. Matter* **1996**, *54*, 16317. [[CrossRef](#)] [[PubMed](#)]
55. Liu, D.; Duan, Y. Structural properties, electronic structures and optical properties of WB<sub>2</sub> with different structures: A theoretical investigation. *Ceram. Int.* **2018**, *44*, 11438–11447. [[CrossRef](#)]
56. Anderson, O. A simplified method for calculating the debye temperature from elastic constants. *J. Phys. Chem. Solids* **1963**, *24*, 909–917. [[CrossRef](#)]
57. Reffas, M.; Bouhemadou, A. Ab initio study of structural, elastic, electronic and optical properties of spinel SnMg<sub>2</sub>O<sub>4</sub>. *Phys. B Condens. Matter* **2010**, *405*, 4079–4085. [[CrossRef](#)]
58. Schreiber, E.; Anderson, O.L.; Soga, N.; Bell, J.F. Elastic Constants and Their Measurement. *J. Appl. Mech.* **1975**, *42*, 747–748. [[CrossRef](#)]
59. Cahill, D.G.; Pohl, R.O. Heat flow and lattice vibrations in glasses. *Solid State Commun.* **1989**, *70*, 927–930. [[CrossRef](#)]
60. Fine, M.E. Elastic constants versus melting temperature in metals. *Scr. Metall.* **1984**, *18*, 951–956. [[CrossRef](#)]

61. Murray, J.L. The CuTi (Copper-Titanium) system. *J. Phase Equilibria* **1983**, *4*, 81–95.
62. Lebedev-Stepanov, P.V. Plasma frequency approach to estimate the Debye temperature of the ionic crystals and metal alloys. *J. Phys. Chem. Solids* **2014**, *75*, 903–910. [[CrossRef](#)]
63. Li, Y.; Ma, X.J. First-principles calculations of the structural, elastic and thermodynamic properties of tetragonal copper-titanium intermetallic compounds. *J. Alloys Compd.* **2016**, *687*, 984–989. [[CrossRef](#)]

**Disclaimer/Publisher’s Note:** The statements, opinions and data contained in all publications are solely those of the individual author(s) and contributor(s) and not of MDPI and/or the editor(s). MDPI and/or the editor(s) disclaim responsibility for any injury to people or property resulting from any ideas, methods, instructions or products referred to in the content.